npj Climate and Atmospheric Science https://doi.org/10.1038/s41612-026-01359-y

Article in Press

Relative roles of different tropical oceans on the weakening of the stratospheric equatorial quasi-biennial oscillation

Received: 20 January 2026

Accepted: 16 February 2026

Cite this article as: Wang, Y., Rao, J., Garfinkel, C.I. *et al.* Relative roles of different tropical oceans on the weakening of the stratospheric equatorial quasi-biennial oscillation. *npj Clim Atmos Sci* (2026). https://doi.org/10.1038/s41612-026-01359-y

Yue Wang, Jian Rao, Chaim I. Garfinkel, Rongcai Ren, Scott M. Osprey & Yixiong Lu

Relative Roles of Different Tropical Oceans on the Weakening of the Stratospheric Equatorial Quasi-Biennial Oscillation

Yue Wang[1], Jian Rao[1]*, Chaim I. Garfinkel[2], Rongcai Ren[3], Scott M. Osprey[4,5]*, Yixiong Lu[6]

[1]State Key Laboratory of Environment Characteristics and Effects for Near-space / Key Laboratory of Meteorological Disaster of Ministry of Education, Nanjing University of Information Science and Technology, Nanjing, Jiangsu 210044, China

[2]Fredy and Nadine Herrmann Institute of Earth Sciences, The Hebrew University of Jerusalem, Edmond J. Safra Campus, Givat Ram Jerusalem 91904, Israel

[3]State Key Laboratory of Numerical Modeling for Atmospheric Sciences and Geophysical Fluid Dynamics (LASG), Institute of Atmospheric Physics, Chinese Academy of Sciences, Beijing, 100029, China

[4]National Centre for Atmospheric Science, Oxford, UK.

[5]Department of Physics, University of Oxford, Oxford, UK.

[6]Earth System Modeling and Prediction Centre, China Meteorological Administration, Beijing 100081, China.

To be submitted to *npj Climate and Atmospheric Science*

*Correspondence: Dr. Jian Rao, raojian@nuist.edu.cn;

Dr. Scott Osprey, scott.osprey@physics.ox.ac.uk

Abstract

The Quasi-Biennial Oscillation (QBO) is the dominant mode of tropical stratospheric variability that modulates global circulation and climate. Although a long-term weakening of QBO amplitude has been observed under global warming, the relative roles of different tropical oceans remain unclear. We perform sensitivity experiments forced by sea surface temperature perturbations over the tropical Pacific, Atlantic, and Indian Oceans, as well as their combined warming, to separate individual and joint effects. Pacific warming produces the strongest weakening and slowest descent of the QBO, whereas Atlantic warming slightly strengthens the amplitude and extends the vertical structure. Indian Ocean warming slightly weakens the amplitude and accelerates the descent. When all three oceans warm simultaneously, the QBO exhibits a weaker amplitude and faster descent, consistent in sign with the combined single-basin responses but with a reduced magnitude owing to diminished zonal and inter-basin SST gradients. Momentum budget analyses further show that basin-dependent competition between equatorial wave forcing and tropical upwelling underlies these contrasting responses.

Keywords: Quasi-biennial oscillation (QBO); Tropical SST warming; wave–mean flow interaction

Introduction

The quasi-biennial oscillation (QBO) is the dominant mode of interannual variability in the tropical stratosphere, characterized by alternating easterly and westerly wind regimes that descend with a mean period of approximately 28 months[1]. The QBO modulates the stratospheric circulation, tracer transport[2], and wave propagation[3], contributing to stratosphere–troposphere coupling and linking tropical variability to extratropical climate[4, 5, 6, 7, 8]. Its high intrinsic predictability makes the QBO a critical source of skill for seasonal-to-decadal climate forecasts[9].

Momentum deposition by equatorially trapped waves drives the QBO[10]. Specifically, eastward shear zones descend primarily through momentum deposition by Kelvin waves and eastward-propagating gravity waves, whereas westward shear zones are sustained chiefly by westward-propagating gravity wave momentum fluxes[11, 12]. The downward propagation is counteracted by tropical upwelling of the Brewer–Dobson (BD) circulation, which transports momentum upward and regulates the QBO period and amplitude[13, 14]. Departures from this balance have been observed in recent years, notably during the disruptions of the descent in 2016 and 2020, when enhanced extratropical wave activity played an important role[15, 16, 17, 18]. Beyond such episodic anomalies, which arise from transient dynamical disturbances, long-term reanalysis records reveal systematic structural changes, with QBO amplitude weakening in the lower stratosphere while strengthening aloft[19]. Progress in simulating the QBO—including higher vertical resolution, extended model tops, and improved gravity wave parameterizations—has enabled more comprehensive assessments of its variability, complementing the limited length and vertical resolution of observational records[20, 21]. Analyses of historical simulations indicate a persistent decline in QBO amplitude in the lower stratosphere, a tendency projected to persist under future warming scenarios[5, 22] (Figure 1).

Understanding and predicting the response of the QBO to global warming has become a central focus of climate research. As greenhouse gas concentrations increase, with CO_2 as the dominant component, a characteristic vertical thermal response develops, marked by tropospheric warming and stratospheric cooling[23]. This vertically coherent thermal adjustment reshapes the stratospheric temperature structure from the tropics to high latitudes, modifying static stability and background winds and thereby influencing wave propagation conditions[24, 25]. At the same time, tropical sea surface temperatures (SSTs) rise[26, 27], reorganizing tropical convection, altering both the generation and spectral characteristics of equatorial waves that deposit momentum to the stratosphere[28, 29]. Global warming also leads to a strengthening of the BD circulation and enhanced tropical upwelling in the lower stratosphere[30], which, together with shifts in equatorial wave forcing has been proposed as a physical explanation for variations in QBO amplitude[19, 31]. This amplitude response is consistently reproduced in climate models, whereas projected changes in the QBO period show little agreement across models and remain poorly constrained[21, 32]. Such inter-model differences in projected QBO period changes are likely linked to contrasting representations of equatorial wave forcing and its coupling with tropical convection and large-scale circulations, including the BD and Walker circulations, under differing realizations of warming across models[33].

Increasing atmospheric CO_2 concentrations and ocean surface warming occur concurrently under global warming, yet they influence the tropical atmosphere through distinct physical pathways. Numerical experiments show that increasing CO_2 tends to suppress tropical precipitation through its direct radiative effect, whereas SST warming invigorates deep convection by increasing atmospheric moisture and radiative cooling[34, 35, 36]. These contrasting responses imply different impacts on tropical wave generation and large-scale circulation. In addition, CO_2-related changes in the BD circulation can be viewed as comprising a direct radiative pathway and

an indirect SST-mediated pathway, with the latter accounting for most of the enhanced tropical upwelling in the lower stratosphere[37]. These differences have prompted efforts to disentangle the respective roles of SST changes and CO_2 increases in shaping QBO variability. Idealized modeling studies indicate that SST warming exerts a dominant influence on changes in QBO amplitude, whereas the direct radiative effects of increased CO_2 in the stratosphere play a comparatively smaller role[38].

Most previous studies have focused on warming applied uniformly across the entire tropical oceans (TO), consistently finding a decrease in QBO amplitude with increasing SST[38, 39]. However, projected SST warming is spatially heterogeneous, and different ocean basins exert distinct influences on tropical convection and wave forcing[40]. Observational and modeling studies indicate that SST variability in the tropical Pacific Ocean (TPO), particularly that associated with the El Niño–Southern Oscillation (ENSO), modulates QBO signals by altering Kelvin and equatorial Rossby wave activity[41]. The QBO-initiative experiments further suggest that QBO periods tend to be longer during La Niña conditions than during El Niño phases[42, 43]. By comparison, the tropical Indian Ocean (TIO) and tropical Atlantic Ocean (TAO) have exhibited rapid warming, which enhances deep convection and can perturb equatorial wave forcing, yet their influence on the QBO remains less well explored. Recent analyses further indicate that correlations between QBO amplitude and SSTs in the western TPO–TIO are considerably stronger than those with the TAO–eastern TPO, underscoring the importance of distinguishing basin-specific contributions[44]. Nevertheless, the underlying mechanisms remain poorly clarified, and the joint versus independent roles of different ocean basins have yet to be systematically assessed.

Here we address this gap with targeted sensitivity experiments using the CESM2–WACCM model. By imposing basin-scale SST anomalies over the TPO, TAO, and TIO separately, as well

as by adding the SST forcing over the TO, we isolate their respective and joint impacts on QBO amplitude, period, and vertical structure. This experimental design enables clear attribution of basin fingerprints, while diagnostics of the zonal momentum budget and residual mean circulation clarify how ocean warming perturbs the balance between wave forcing and tropical upwelling, thereby providing a physically grounded framework for interpreting QBO responses in future climates characterized by spatially heterogeneous SST warming. This framework also provides a useful perspective for interpreting how differences in simulated SST warming patterns across models may contribute to divergent QBO period responses. Together, these analyses advance understanding of how the QBO responds to global warming and its implications for climate prediction.

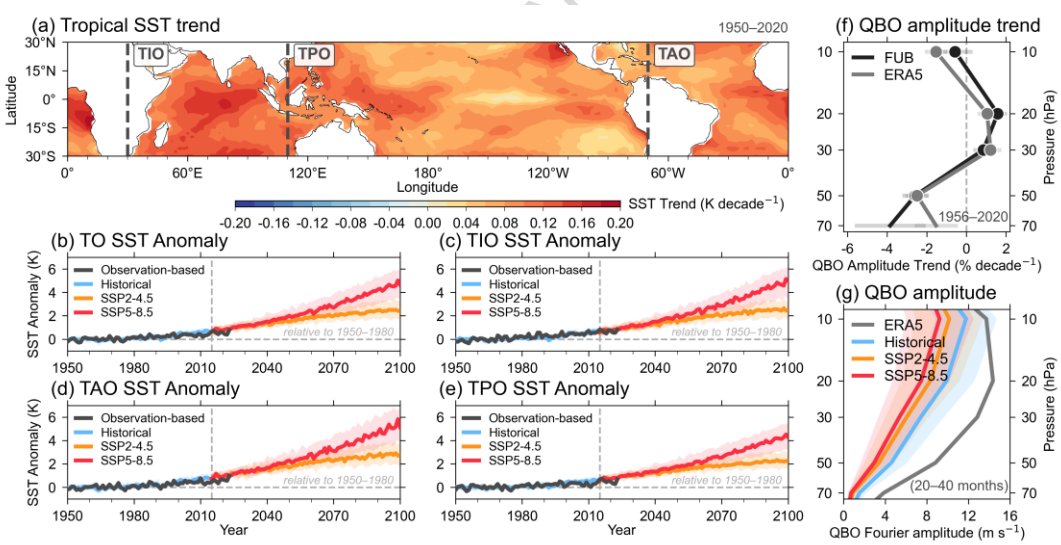

Figure 1. Tropical SST evolution and QBO amplitude responses (a) Multi-dataset mean tropical SST trends (30° S–30° N) for 1950–2020 derived from observational SST datasets (COBE-SST, HadISST and ERSST) together with the ERA5 reanalysis. (b–e) SST anomalies relative to the 1950–1980 climatology averaged over the tropical oceans (TO), tropical Indian Ocean (TIO), tropical Atlantic Ocean (TAO) and tropical Pacific Ocean (TPO), shown for observation-based datasets and CMIP6 multi-model means from historical simulations (1950–2014) concatenated with SSP2-4.5 and SSP5-8.5 projections (2015–2100). (f)

Vertical profiles of linear trends in QBO amplitude (% decade^{-1}) using zonal winds averaged over 5° S–5° N from the ERA5 reanalysis and FUB observations for 1956–2020. (g) Vertical distribution of QBO amplitude using zonal winds averaged over 5° S–5° N, derived from 20–40-month band-pass-filtered zonal-mean zonal wind power spectra for ERA5 and the CMIP6 multi-model mean. Shading shows ±2 standard errors of the multi-model mean; error bars on black curves indicate ranges significant at the 95% level.

Results

Simulation of the QBO

To provide a foundation for analyzing the impacts of tropical ocean warming, we first evaluate how well CESM2-WACCM reproduces the observed QBO in its control (CTRL) simulation. The model can generally capture the oscillation characteristics, with alternating easterly and westerly shear zones propagating downward through the equatorial stratosphere (Figure 2a). The simulated oscillation retains the observed asymmetry between easterly and westerly phases, with average peak amplitudes of −29m s^{-1} and 11 m s^{-1} in CTRL compared with −35 m s^{-1} and 15 m s^{-1} in ERA5.

Spectral analyses of equatorial zonal winds reveal dominant power in the quasi-biennial band, with secondary peaks at annual and semiannual timescales in both datasets (Figures 2 b and d). The simulated QBO exhibits a period range of 24.0–35.8 months (mean: 28.8 months), closely matching the ERA5 range of 22.9–34.7 months (mean: 28.6 months). These differences are small relative to the intrinsic variability of the oscillation. The spatial distribution of variance is characterized by a symmetric meridional profile centered on the equator, as revealed by Fourier amplitudes, with CTRL producing a slightly narrower extent and a weaker peak amplitude (Figures 2 c and e). In the vertical dimension, both ERA5 and CTRL exhibit maximum amplitudes near 20 hPa, with coherent signals extending from approximately 10 hPa to 70 hPa. The CTRL simulation,

however, shows a somewhat shallower descent of alternating wind regimes into the lowermost stratosphere, suggestive of weaker vertical momentum transport.

Overall, CESM2-WACCM reproduces the essential observed characteristics of the QBO—including its oscillatory structure, temporal scale, and spatial morphology—providing a reliable baseline for assessing how tropical SST warming modulates QBO dynamics.

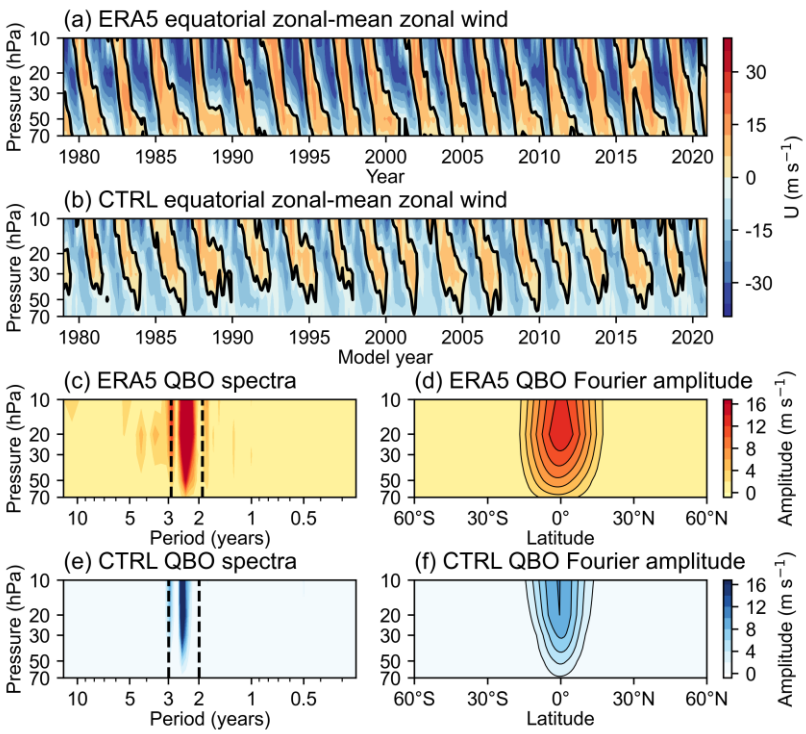

Figure 2. Comparison between the observed and simulated QBO structure. Time–pressure section of monthly mean equatorial (5°S–5°N) zonal mean zonal winds (m s^{-1}) from ERA5 (a) and the CESM2-WACCM control (CTRL) simulation (b), with the zero-wind contour highlighted. (c, e) Power spectra of equatorial zonal winds in ERA5 and CTRL, respectively. Vertical dashed lines indicate the dominant QBO periodicity band. (d, f) Latitude–pressure structure of QBO Fourier amplitude in ERA5 and CTRL, defined as the square root of spectral power summed within the QBO band and normalized by total variance.

QBO responses to tropical SST warming

Building on the CTRL simulation as a baseline, we design four sensitivity experiments to quantify QBO responses to tropical SST warming: a pan-tropical warming case (TO) with the SST warming trend (1950-2020) imposed across all tropical basins, and three single-basin SST perturbations over the TPO, TAO, and TIO. In the single-basin experiments, only SST in the designated ocean basin is perturbed while the others remain at the CTRL climatology (forced by the observed 1950-1980 mean SST), thereby isolating each basin's individual contribution to QBO variability. Figure 3 shows the prescribed SST forcings based on the 1950-2020 SST trend. The observed SST trend anomalies display pronounced regional contrasts, with stronger warming in the western-TPO and TIO and weaker increases in the TAO and eastern-TPO, forming a west–east gradient reminiscent of a La Niña–like state.

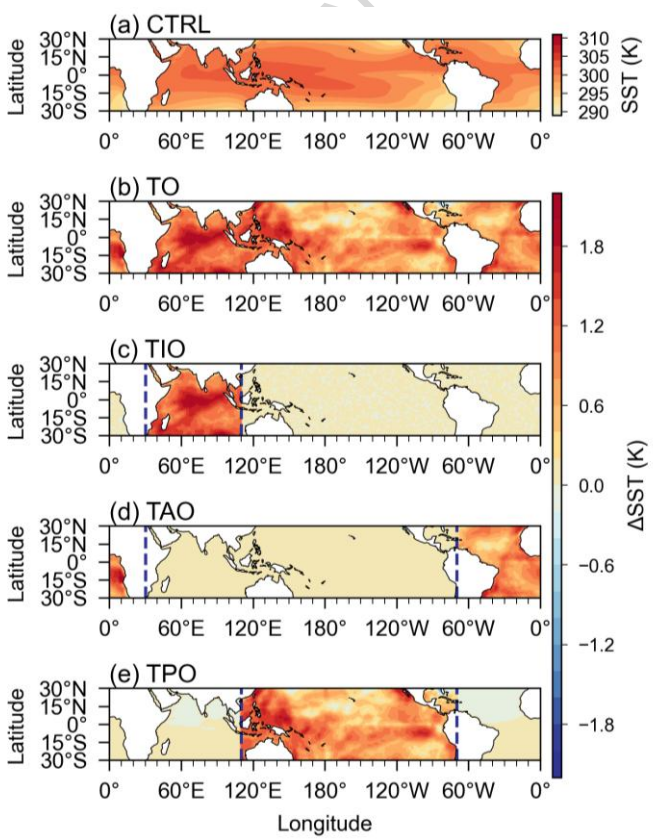

Figure 3. Prescribed SST forcing fields. Spatial patterns of SSTs used in the experiments. (a) Climatological (1950-1980) SSTs in the control simulation (CTRL). (b–e) Basin-scale SST trend anomalies

relative to CTRL for pan-tropical warming (TO; b) and single-basin forcings over the Indian Ocean (TIO; c), Atlantic Ocean (TAO; d), and Pacific Ocean (TPO; e).

In all experiments, the leading two empirical orthogonal functions (EOFs) preserve the canonical quadrature-phase vertical structures of the QBO, explaining over 90% of the variance (Figures 4a and b). The corresponding principal component trajectories in the PC1–PC2 phase space remain quasi-circular, confirming that the oscillation still persists as a coherent cyclic mode despite imposed warming (Figure 4c). This robustness allows us to employ an EOF-based phase definition, dividing each cycle into eight phases aggregated into four dynamical stages—westerly shear (P1–P2), westerly core (P3–P4), easterly shear (P5–P6), and easterly core (P7–P8), with reference to the vertical QBO structure and the characteristic wind shear near ~30 hPa (Figure 5).

The role of SSTs in each basin for the QBO modulation emerges prominently in the EOF-based amplitude and period distributions (Figures 4d and e). In the CTRL run, the mean amplitude is 19.9 m s^{-1} with a period of 29.6 months, and easterly core phases exhibit stronger amplitudes than westerly core phases. Responses to warming in each basin diverge substantially: The TPO run produces the strongest weakening across all phases, with the mean amplitude reduced to 10.5 m s^{-1} (about half of CTRL) and the period extended to 38.5 months. Additionally, the period lengthening is particularly pronounced during easterly shear phases. In contrast, the TAO run is the only case in which the oscillation is strengthened, with the amplitude increased to 21.5 m s^{-1} and the mean period decreased to 25.6 months (i.e., a faster cycle). The TIO SST forcing exerts a weaker influence, and the TIO run produces an amplitude of 16.6 m s^{-1} and a comparable 26.5-month period. In the TO run, the amplitude drops to 17.8 m s^{-1} and the period shortens to 26.3 months, showing the same qualitative tendency as indicated by the individual basin responses, but with a muted overall magnitude.

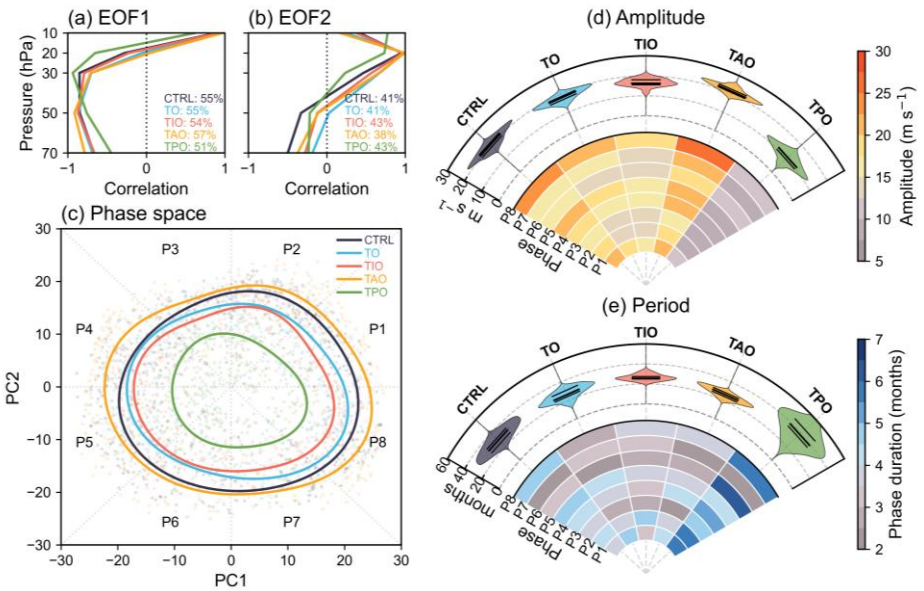

Figure 4. Comparison of QBO responses under pan-tropical and basin-specific SST warming. (a, b) First two EOFs of equatorial (5°S–5°N) deseasonalized zonal mean zonal winds for CTRL, TO, TIO, TAO and TPO runs (70–10 hPa; 504 months). (c) Phase-space trajectories from the timeseries (PC1 and PC2) of the first two EOFs in a and b. (d) QBO EOF-based amplitude: heatmap indicates phase-mean amplitude (m s^{-1}) for Phases 1–8, and violin plots show the distribution of cycle-mean amplitude for each experiment (lines mark the 25th, 50th and 75th percentiles). (e) QBO period: heatmap indicates phase-mean duration (months), and violin plots show the distribution of cycle-mean period (25th, 50th and 75th percentiles). See the methods for details.

Phase composites of equatorial zonal wind (Figure 5) further reveal structural differences. All experiments reproduce the canonical downward propagation of the QBO: westerlies first appear in the upper stratosphere at P1 and gradually propagate downward, reaching the lower levels by P4. Similarly, easterlies develop from P5 and propagate downward to the lower stratosphere by P8. Among the experiments, the TPO run exhibits the largest departure from CTRL. The shear zones are substantially weakened, with amplitudes markedly reduced in the upper stratosphere and nearly absent below 50 hPa, accompanied by a diminished asymmetry between easterly and

westerly phases. In addition to this amplitude reduction, the TPO run displays a distinct phase delay relative to CTRL, with transition points systematically shifted toward later phases (Figure S1). By contrast, the TAO run shows an opposite but weaker adjustment, with slightly stronger amplitudes and enhanced vertical shear, in contrast to the reduced QBO amplitudes in the TPO run. The TO and TIO runs, however, show only modest departures from CTRL, with weaker amplitudes but similar vertical structure or phase progression.

The QBO exhibits varied responses to SST warming in different tropical ocean basins, with distinct amplitude, period, and structural changes. Notably, the TO experiment applies a synchronized SST perturbation constructed from the basin-scale SST trends used in TPO, TIO, and TAO. The resulting QBO response follows the same qualitative tendency as implied by the three single-basin experiments, but its magnitude is not additive, consistent with the reduced zonal and inter-basin SST gradients under simultaneous warming.

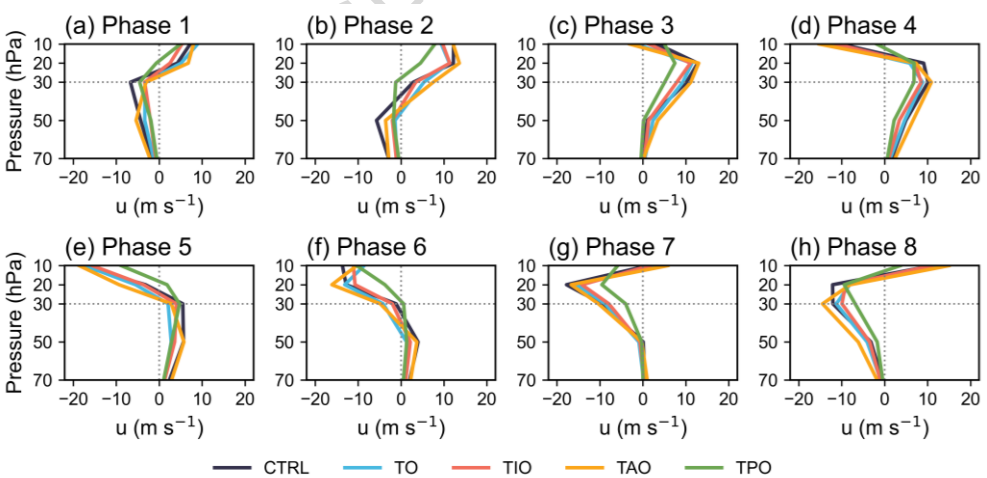

Figure 5. Phase-composite QBO structures under pan-tropical and basin-specific SST warming. Panels (a–h) show equatorial (5°S–5°N, 70–10 hPa) deseasonalized zonal mean zonal winds composited into eight QBO phases for CTRL, TO, TIO, TAO and TPO runs. Phases are defined from the principal-component phase angle and grouped into four dynamical stages: westerly shear (P1–P2), westerly core (P3–P4), easterly shear (P5–P6) and easterly core (P7–P8).

Dynamical drivers of QBO variability: Momentum budget analysis

The structural changes of the QBO raise a question: Which dynamical processes are responsible for the basin sensitivity of the QBO changes? We diagnose the zonal wind balance using the transformed Eulerian-mean framework. Key contributors to the zonal-mean zonal-wind tendency include resolved wave forcing (denoted by Eliassen–Palm flux divergence), parameterized gravity-wave drag (GWD), and vertical advection by the residual mean circulation ($-\bar{w}^{*}\partial\bar{u}/\partial z$) (Figures 6 and S2)[45].

In the CTRL run (Figure 6a), resolved wave forcing and GWD alternate as the dominant westerly and easterly momentum sources that peak within the shear zones. Vertical advection provides a westerly tendency within easterly shear zones, consistent with residual upwelling opposing the downward descent of the easterly shear. All these terms sustain the alternating shear structure and control the descent of QBO phases.

In the TPO run (Figure 6e), the zonal momentum budget terms are significantly weakened for nearly all phases. The reduction in GWD is most pronounced, particularly during the descent of easterly shear zones. In the upper stratosphere, the peak easterly GWD shifts to later phases and is strongly reduced, with the easterly peak at 20 hPa weakened by about 74% relative to CTRL. This substantial reduction diminishes the usual asymmetry between easterly and westerly GWD forcing. This might imply that penetration and dissipation of westward-propagating gravity waves is reduced in the upper stratosphere, which in turn diminishes easterly momentum deposition and slows the downward progression of easterly shear. In the lower stratosphere, by contrast, the alternating momentum signals below 50 hPa in CTRL are almost absent in TPO. The contribution from resolved wave forcing is smaller than that from GWD. During westerly shear phases its positive tendency is substantially reduced relative to CTRL, comparable in magnitude to the GWD

reduction. However, during easterly shear phases, easterly momentum forcing is nearly unchanged in TPO vs CTRL. Vertical advection also exhibits level-dependent changes: it strengthens and persists in the 10–20 hPa layer during easterly shear phases, thereby opposing the downward propagation of QBO anomalies, while below 50 hPa it remains comparatively weak. The combined effect of reduced GWD, weaker resolved wave forcing, and enhanced upper-level vertical advection confines maximum easterly cores above ~30 hPa, decreases QBO amplitudes, and prolongs easterly phases, consistent with the extended cycles shown in Figure 4. These features explain why TPO produces the strongest weakening and delay among all experiments, whereas the responses in other basins are weaker or even opposite.

The TAO warming induces a moderate strengthening of the QBO momentum budget terms (Figure 6d). Both resolved wave forcing and GWD are slightly enhanced relative to CTRL, and the alternating momentum anomalies penetrate to deeper depth, thereby facilitating a more effective phase descent. Vertical advection also increases, though the magnitude of the change remains comparatively small: At 30 hPa during easterly shear phases, the positive tendency from vertical advection reaches only about one third of the negative tendency associated with GWD. Hence, TAO warming yields slightly shorter periods and stronger shear zones that extend deeper than in CTRL.

The QBO and the associated momentum budget terms in TO and TIO are comparable to CTRL (Figures 6b and c). In both runs, GWD in the upper stratosphere is reduced—at 20 hPa the easterly GWD maximum decreases by about 32% in TO and 26% in TIO—and the resolved wave forcing during westerly shear phases is likewise weaker than in CTRL. Below 50 hPa, the alternating momentum signals evident in CTRL are largely absent, and wind tendencies are predominantly negative. The vertical advection term that opposes the downward propagation of

shear is also weaker than in CTRL, further reducing resistance to phase descent. Consequently, shear zones descend more rapidly, QBO amplitudes are reduced, and the period shortens.

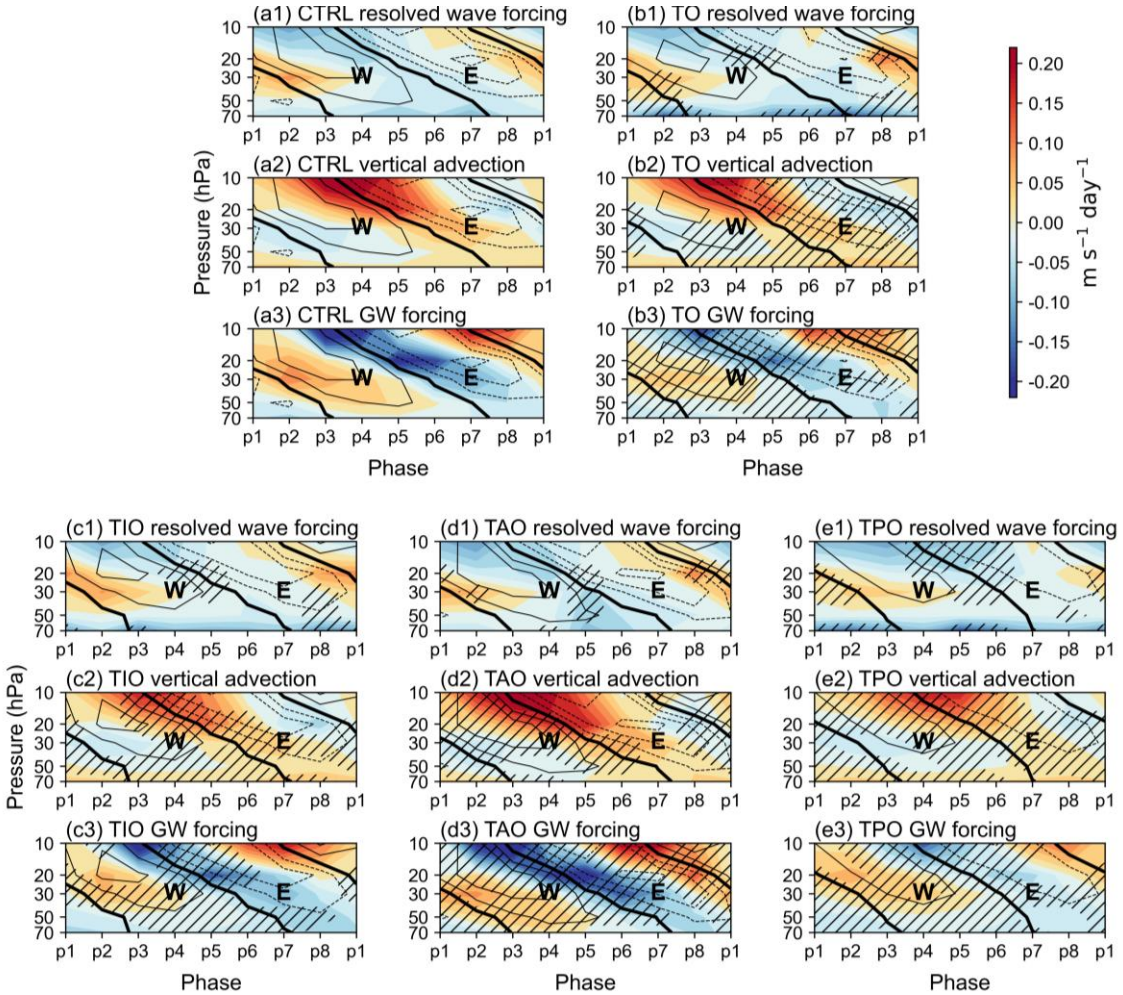

Figure 6. Momentum budget analysis of the QBO under pan-tropical and basin-specific SST warming. Panels (a–e) show phase–height composites (5°S–5°N, 70–10 hPa; P1–P8) of zonal-momentum tendencies for CTRL, TO, TIO, TAO and TPO: resolved wave forcing (Eliassen–Palm flux divergence), parameterized gravity-wave drag (GWD) and vertical advection. Shading denotes tendencies (m s^{-1} day^{-1}). Black contours denote zonal-mean wind (5 m s^{-1} intervals; thick contour = 0). Hatching denotes regions significantly different from CTRL at the 95% confidence level.

To further clarify the role of residual advection, we examine the residual vertical velocity ($\bar{w}^*$), which provides a direct diagnostic of tropical upwelling, shown in Figure 7. The upwelling

($\bar{w}^*$) in CTRL is small in the lower stratosphere (70–50 hPa, ~0.15 mm s^{-1}) and increases with height, reaching maxima of 0.5 mm s^{-1} at 10 hPa. At 10 hPa during P5–P8, TPO maintains larger $\bar{w}^*$—from 0.72 to 0.29 mm s^{-1}—than CTRL (from 0.59 to 0.18 mm s^{-1}). By contrast, TAO has the weakest $\bar{w}^*$ at this level, reaching only 0.05 mm s^{-1} at P7, the minimum among all experiments. At 20–30 hPa, TPO exhibits smaller $\bar{w}^*$ than the other experiments, indicating a level-dependent redistribution of residual upwelling (Figure S3). In the lower stratosphere, both $\bar{w}^*$ and vertical shear are weak, so the residual advection contribution to the momentum budget is limited. Taken together, these diagnostics show that the inter-experiment differences are produced primarily through the persistence and altitude of upper-level upwelling, rather than through changes below 50 hPa.

Therefore, basin-dependent contrasts emerge from the combined influence of wave-driven momentum deposition and residual upwelling, which together determine how tropical SST warming reshapes the stratospheric QBO response.

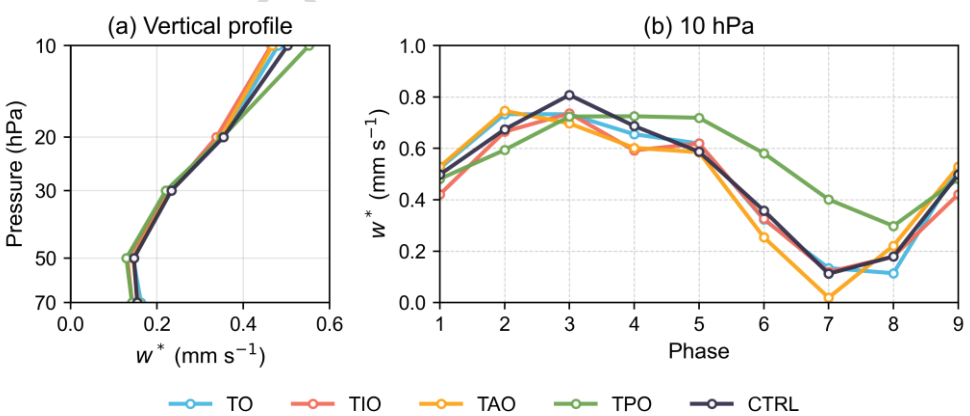

Figure 7. Residual vertical velocity ($\bar{w}^*$, mm s^{-1}) associated with tropical upwelling. (a) Phase-averaged vertical profiles (5°S–5°N, 70–10 hPa). (b) Phase evolution at 10 hPa (P1–P8) for CTRL, TO, TIO, TAO, and TPO.

Tropical ocean warming as a modulator of QBO dynamics

Why do the TEM momentum budget terms respond differently under distinct SST-warming patterns? In the real atmosphere, the wave momentum flux entering the stratosphere is determined by two coupled pathways: (i) adjustments of convective wave sources, and (ii) modifications of the propagation environment (background wind, temperature, static stability), which together determine where waves are filtered, refracted, and ultimately dissipate.

The equatorial precipitation climatology indicates the convective wave source strength (Figure 8). Among the SST-perturbation experiments, the TAO run maintains the largest equatorial maximum rainfall (Figure 8c), consistent with an active convective source near the Equator. By contrast, TPO exhibits a marked reduction of precipitation within 5°S–5°N and a northward-displaced intertropical convergence zone (ITCZ), with precipitation between 5°–30°N exceeding that in the other experiments (Figure 8c). Because off-equatorial convection projects less efficiently onto symmetric equatorial wave modes, this redistribution weakens the effective equatorial waves that carry momentum flux and enter the equatorial stratosphere.

Relative to the TAO run, the TPO run is characterized by tropospheric warming and lower-stratospheric cooling, which raises the tropopause and changes the static stability: N^2, the square of the buoyancy frequency, is reduced in the tropopause layer but enhanced above (Figure S4). This vertical structure enables the tropopause to be more permeable to deep convection while suppressing vertical wave propagation into the middle stratosphere, shifting the level of momentum dissipation upward. Concurrent circulation adjustments (Figures 8a and b) reinforce these contrasts: TPO warming strengthens the Walker overturning with enhanced ascent over the Maritime Continent–western Pacific and stronger descent over the eastern Pacific, whereas TAO exhibits a weaker Walker cell. Because Walker circulation acts as a filter for gravity waves propagating from the troposphere into the stratosphere, a weaker Walker circulation may reduce

such filtering and allow more waves to reach the stratosphere[46, 47]. By contrast, the deepened overturning under TPO warming intensifies upper-tropospheric westerlies (~150–100 hPa) and modifies the location of critical layers for equatorial waves, to increase background filtering and absorption before waves can reach the stratosphere. In aggregate, these thermal dynamical changes diminish the momentum flux and elevate the momentum deposition height by equatorial waves.

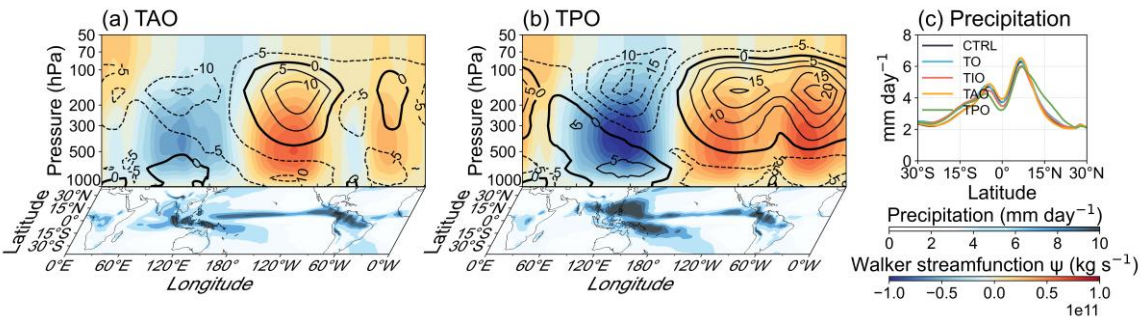

Figure 8. Basin-scale thermodynamic contrasts under pan-tropical and basin-specific SST warming. (a–b) Longitude–pressure cross-sections of the climatological Walker stream function (kg s^{-1}, shading) with zonal wind contours (5 m s^{-1} intervals; thick line = 0), overlaid with climatological precipitation (mm day^{-1}, latitude–longitude fields) for TAO (a) and TPO (b). (c) Zonal-mean climatological precipitation (mm day^{-1}) averaged over 30°S–30°N for CTRL, TO, TIO, TAO and TPO.

Different from the contrasting TAO and TPO responses, the TIO and TO experiments show moderate behaviors: the Walker circulation also becomes somewhat stronger than in CTRL, but this enhancement coincides with weaker equatorial convective wave sources. The competing influences between TAO vs TPO lead to QBO responses that fall between the pronounced weakening under TPO and the moderate strengthening under TAO: amplitudes are reduced and periods shortened, though the changes remain closer to CTRL (Figure S5).

In short, the modeling evidence shows that tropical SST warming modulates QBO dynamics through two coupled pathways: adjustments of convective wave sources and changes in the

propagation and filtering environment, jointly influencing where momentum is deposited and the rate of phase descent.

Discussion

The QBO is a fundamental component of tropical–extratropical coupling and a key source of subseasonal-to-seasonal predictability[48]. Previous studies have primarily emphasized rising atmospheric CO_2 concentrations and increases in global-mean SST under a warming climate as key influences, showing that both can alter the balance between tropical upwelling and wave-driven momentum deposition[1, 44]. However, the influence of SST warming, particularly its sensitivity to basin-scale spatial structure, has remained insufficiently quantified. Here, basin-targeted SST perturbation experiments allow us to isolate and quantify the contributions of SST warming in individual tropical basins, revealing distinct basin-specific signatures in the QBO response (Figure 9). TPO warming produces the strongest weakening, with elevated easterly cores, reduced QBO amplitudes, and longer cycles; TAO warming modestly strengthens the oscillation and shortens its period; TIO warming yields an intermediate state of weaker amplitude but faster descent. In the synchronized warming case (TO), the QBO response exhibits the same qualitative tendency as that inferred from the three individual basin experiments, with reduced amplitudes and shorter cycles. These contrasts underscore the importance of basin-scale SST spatial structure for QBO adjustment, beyond changes in tropical-mean or global-mean SST alone.

The TEM momentum budget clarifies the dynamics behind these patterns. Under TPO warming, the overall momentum forcing is weakened, consistent with the marked reduction in QBO amplitude and lengthening of its cycle. Both GWD and resolved EP-flux divergence decrease in strength, with the most pronounced change during easterly phases in the upper stratosphere,

where momentum deposition is delayed and confined to higher altitudes. Residual upwelling also persists aloft (~10–20 hPa), further opposing the downward progression of shear zones. Under TAO warming, robust near-equatorial convection and weaker Walker filtering sustain both parameterized and resolved wave momentum tendencies and permit deeper penetration of alternating shear, yielding slightly larger amplitudes and shorter cycles. Under TIO warming, the reduction in upper-level GWD and resolved forcing is accompanied by weak residual vertical advection below 50 hPa, allowing shear zones to descend more quickly despite their smaller amplitudes. In the TO run, diminished upper-level GWD, muted alternation below ~50 hPa, and weaker residual upwelling than in CTRL combined to produce reduced amplitude. The TO response reflects competing wave–mean-flow adjustments induced by TAO, TPO, and TIO warming. However, simultaneous warming across the three basins reduces both zonal and inter-basin SST gradients, weakening the dynamical contrasts that are pronounced in the single-basin experiments and thereby limiting the response magnitude while preserving its overall sign.

Our basin-scale experiments connect directly with previous evidence on the drivers of QBO variability. Observational analyses and reanalyses have shown that ENSO strongly modulates QBO descent: El Niño events tend to accelerate phase progression, whereas La Niña slows it, through changes in convection and mean-flow filtering[46, 47]. The TPO response in our experiments is dynamically consistent with this La Niña-like modulation, exhibiting weaker equatorial convection, a strengthened Walker circulation, and enhanced upper-tropospheric westerlies that raise the level of gravity wave dissipation and prolong easterly phases. This behavior is also consistent with the recently observed La Niña-like tropical SST trend pattern[49, 50]. By contrast, the modest strengthening of QBO amplitude under TAO warming has been comparatively less explored in earlier literature, yet it accords with evidence highlighting the Atlantic's role in

sustaining equatorial convection and Kelvin wave activity[51, 52]. We emphasize that this strengthening should be interpreted as a relative adjustment to a basin-specific forcing, rather than a contradiction of the well-documented long-term weakening of QBO amplitude in both observations and future projections[5, 19]. The weaker adjustment under TIO warming is consistent with its reduced projection onto equatorial modes. Collectively, these results clarify why synchronized warming experiments consistently report robust amplitude reductions but divergent period changes. The amplitude response is robust because warming in all basins except for TAO acts to diminish equatorial wave sources or elevate their dissipation levels, thereby reducing the overall momentum available to sustain alternating shear zones[53]. By contrast, differences in period arise from how basin-specific SST forcings modify the net balance between wave-driven momentum deposition and residual tropical upwelling. This dynamical framework is also supported by multi-model assessments that attribute spread in QBO projections to variations in gravity wave parameterizations, vertical resolution, and tropical upwelling trends[45, 54].

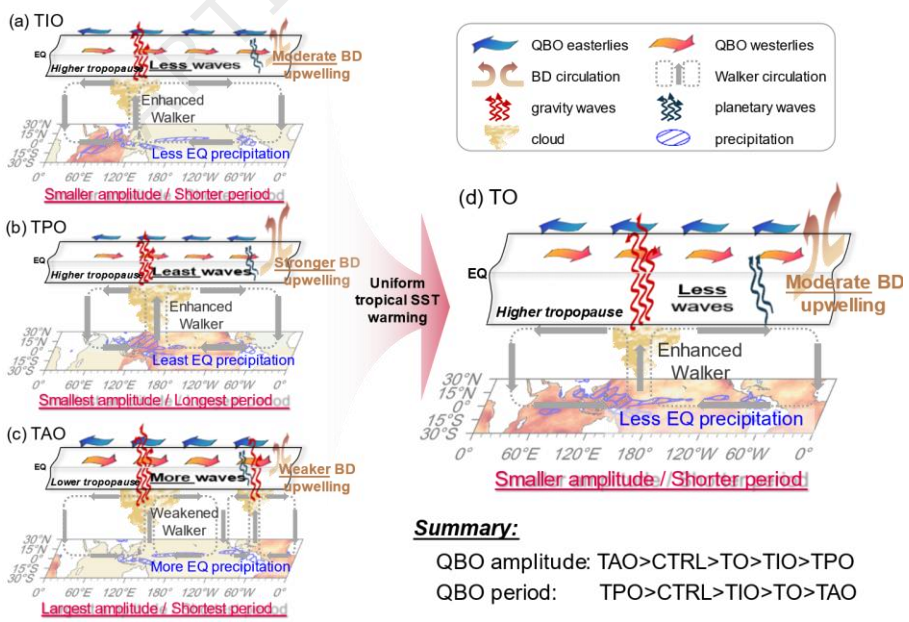

Figure 9. Schematic mechanisms of QBO responses to tropical ocean warming. (a–c) Responses to

single-basin warmings over the TIO, TPO, and TAO; (d) pan-tropical synchronized warming (TO). All variations are shown relative to the CTRL run.

Several limitations must be acknowledged. First, the experiments rely on a single model (CESM2-WACCM) whose gravity-wave parameterizations and vertical resolution may not fully capture the spectrum of equatorial wave forcing. Second, the design isolates basin SST warming but does not incorporate other forcings, such as aerosols, volcanic eruptions, or extreme ENSO events, which can also perturb the QBO. Finally, the large internal variability of the QBO implies that ensemble sizes beyond those used here are needed to quantify the robustness of basin fingerprints. These caveats underscore that our results should be interpreted as process-based insights rather than precise forecasts.

Building on these findings, a clearer picture emerges of how tropical SST warming can inform future QBO prediction. By identifying basin-specific fingerprints of wave forcing and upwelling, our results provide a framework for improving the representation of the QBO, thereby reinforcing the QBO as a reliable source of predictability for subseasonal-to-seasonal and decadal subseasonal-to-seasonal and decadal climate forecasts. This perspective also helps place recent QBO disruption events in context: the interruptions in 2016 and 2020, linked to extratropical wave activity, illustrate how departures from the canonical wave mean flow balance can override the oscillation[15, 18, 55, 56]. Understanding how basin-scale SST anomalies precondition this balance may improve our ability to anticipate such cut-off events. Looking ahead, coupling basin-pattern indices with ENSO phase and real-time wave-activity diagnostics within probabilistic, ensemble frameworks offer a practical path to conditional QBO forecasts. Incorporating coupled feedback and explicitly accounting for large internal variability will be essential to translate these mechanistic insights into robust guidance under continued ocean warming.

Methods

Data

We use three observational datasets to derive sea surface temperature (SST) trends: HadISST1 provided by the Met Office Hadley Centre[57], ERSST version 5 provided by the National Oceanic and Atmospheric Administration[58], and COBE-SST2 (COBE2) provided by the Japan Meteorological Agency[59]. Monthly SST fields from HadISST1 and COBE2 are originally available on a 1° × 1° latitude–longitude grid, whereas ERSST v5 has a native resolution of 2° × 2°. To ensure consistency across datasets, all SST fields are interpolated onto a common 2° × 2° grid prior to analysis, and trends are computed over a common analysis period from 1950 to 2020.

We use monthly mean radiosonde data of equatorial zonal wind from three stations, Canton Island, Gan/Maledive Islands, and Singapore, provided by Freie Universität Berlin (FUB) dataset, covering the period 1956–2020[60], together with reanalysis data, to evaluate the vertical structure and temporal evolution of the QBO. Reanalysis fields are taken from the ECMWF fifth generation reanalysis (ERA5), which has a horizontal resolution of approximately 0.25° and 137 vertical levels extending up to 0.01 hPa (80 km)[61]. To compare with our model output, we use 6-hourly sampling interpolated to a 1° × 1° grid and 27 pressure levels.

We use monthly-mean outputs from the Coupled Model Intercomparison Project Phase 6 (CMIP6) experiments, including historical simulations for 1950–2014 and future projections under the SSP2-4.5 and SSP5-8.5 scenarios for 2015–2100[62]. A total of 14 CMIP6 models that simulate a QBO-like oscillation are included in the analysis, namely AWI-CM-1-1-MR, BCC-CSM2-MR, CESM2-WACCM, CNRM-CM-6-1, CNRM-ESM2-1, EC-Earth3, EC-Earth3-Veg, GFDL-ESM4, HadGEM3-GC31-LL, IPSL-CM6A-LR, MIROC6, MPI-ESM1-2-HR, MRI-ESM2-0, and UKESM1-0-LL. Details of the models used in this study are summarized in Supplementary Table

S1, including their institutional affiliation, horizontal resolution, number of vertical levels, and the atmospheric model top.

Model description and experiments

We use the Whole Atmosphere Community Climate Model version 6 (WACCM6), a stratosphere-resolving atmospheric general circulation model that forms part of the Community Earth System Model version 2 (CESM2) developed by the National Center for Atmospheric Research (NCAR)[63]. The model extends from the surface up to ~140 km altitude, with a horizontal resolution of 0.95° latitude × 1.25° longitude.

We conducted five experiments to investigate the atmospheric responses to regional tropical sea surface temperature (SST) anomalies, comprising a control simulation (CTRL) and four sensitivity experiments[64, 65]. The CTRL experiment is forced by the climatological annual cycle of monthly SSTs derived from the period 1950–1980, i.e., SST varies with calendar month but remains constant across years. This simulation is integrated for 52 years, with the final 51 years used to establish a reference state of atmospheric circulation in the absence of imposed SST anomalies. The four sensitivity experiments impose SST trend anomalies (during 1950–2020) over specific tropical ocean domains to isolate the impacts of regional SST forcing, and each experiment is integrated for 52 years, with the final 51 years used for analysis, consistent with CTRL. The SST trend anomalies are applied within the following regions: the entire tropics (30°S–30°N, 0°–360°; TO), the tropical Pacific Ocean (110°E–70°W; TPO), the tropical Indian Ocean (30°E–110°E; TIO), and the tropical Atlantic Ocean (70°W–30°E; TAO). Outside these forcing regions, SSTs follow the climatological seasonal cycle as in the CTRL simulation. Statistical significance of differences relative to CTRL is evaluated using a two-sided t test at the 95% confidence level.

EOF-based QBO phase space

The QBO phase progression is characterized in a two-dimensional phase space constructed from empirical orthogonal function (EOF) analysis[66, 67]. Monthly equatorial zonal-mean zonal winds (10–70 hPa) are deseasonalized, and an EOF decomposition is performed. The leading two modes, which together explain over 90% of the total variance, are retained. For the reanalysis-based EOF analysis, the 2015/16 and 2019/20 QBO disruption events are excluded to avoid interference from anomalous phase evolution. The QBO state is then represented by its principal components (PC_1 and PC_2), defining an instantaneous amplitude (*Amp*) and phase angle (φ) in phase space as: $Amp = \sqrt{\mathrm{PC}_1^2 + \mathrm{PC}_2^2}, \varphi = \arctan(\mathrm{PC}_2/\mathrm{PC}_1)$.

To examine the phase-dependent evolution of the QBO, the phase trajectory is partitioned into eight equal angular sectors (–180° to 180° in 45° intervals), consistent with previous studies. Variables are composited within each phase bin across all QBO cycles to construct phase-resolved composites of zonal-mean winds and wave-forcing fields.

Momentum budget analysis

To elucidate the dynamical drivers of QBO variability, we analyze the zonal mean zonal momentum budget using the transformed Eulerian mean (TEM) formulation in spherical geometry with log-pressure coordinates[68, 69, 70]:

$$\frac{\partial \overline{u}}{\partial t} = \left(f - \frac{1}{a\cos\phi}\frac{\partial}{\partial \phi}(\overline{u}\cos\phi) \right)\bar{v}^* - \overline{w}^*\frac{\partial \overline{u}}{\partial z} + \frac{1}{\rho_0 a\cos\phi}\nabla \cdot \boldsymbol{F} + \overline{X}. \qquad (1)$$

The left-hand side represents the zonal mean zonal wind tendency, balanced by three distinct processes on the right-hand side: momentum advection by the residual circulation, wave-induced momentum forcing, and sub-grid-scale processes. The first two terms describe meridional and vertical advection by the residual circulation components $\bar{v}^*$and $\overline{w}^*$are defined as:

$$\bar{v}^* = \overline{v} - \frac{1}{\rho_0}\left(\frac{\rho_0 \overline{v'\theta'}}{\overline{\theta_z}}\right)_z, \tag{2}$$

$$\overline{w}^* = \overline{w} + \frac{1}{a\cos\phi}\left(\cos\phi\ \frac{\overline{v'\theta'}}{\overline{\theta_z}}\right)_\phi. \tag{3}$$

The third term quantifies the momentum deposition by resolved waves, expressed as the divergence of the Eliassen–Palm (EP) flux:

$$\nabla \cdot \mathbf{F} = \left[\frac{1}{a\cos\phi}\frac{\partial}{\partial\phi}\left(F_\phi \cos\phi\right) + \frac{\partial F_z}{\partial z}\right], \tag{4}$$

where the meridional (F_ϕ) and vertical (F_z) components of the EP flux are given by:

$$F_\phi = \rho_0 a\cos\phi\left(\frac{\overline{v'\theta'}}{\overline{\theta_z}}\,\overline{u_z} - \overline{v'u'}\right), \tag{5}$$

$$F_z = \rho_0 a\cos\phi\left(\frac{\overline{v'\theta'}}{\overline{\theta_z}}\left(f - \frac{1}{a\cos\phi}(\overline{u}\cos\phi)_\phi\right) - \overline{w'u'}\right). \tag{6}$$

The final term, $\overline{X}$, represents sub-grid-scale momentum sources and sinks, primarily arising from parameterized gravity wave drag (GWD) and numerical diffusion, which are essential in maintaining the QBO, where resolved wave forcing becomes insufficient.

In these expressions, *u, v* and *w* denote the zonal, meridional, and vertical wind components, respectively, and θ is potential temperature. The overbar indicates a zonal mean, and the prime denotes deviations from the mean. The variables ρ_0, *a*, ϕ, *z,* and *f* represent the log-pressure height-dependent air density, Earth's radius, latitude, log-pressure height, and Coriolis parameter ($f = 2\Omega\sin\phi$), respectively. The subscripts ϕ, *z*, and *t* denote the meridional, vertical, and time derivatives, respectively.

Estimation of Walker circulation

The Walker circulation is quantified using the zonal mass stream function (Ψ), defined as[71]:

$$\psi = 2\pi a \int_0^p u_D\ \frac{dp}{g}, \tag{7}$$

where g is gravitational acceleration, and u_D is the divergent component of the zonal wind, averaged over the zonal band from 5°S to 5°N, while other parameters follow the definitions above. The integral is evaluated over pressure (p), from the top of the atmosphere to the surface, yielding the zonal mass flux per unit latitude circle. Ψ serves as a diagnostic of the strength of equatorial zonal overturning circulation, particularly over the Pacific sector.

Data availability

The SST datasets are available from HadISST1 (https://hadleyserver.metoffice.gov.uk/hadisst/data/download.html), ERSST v5 (https://psl.noaa.gov/data/gridded/data.noaa.ersst.v5.html) and COBE2 (https://psl.noaa.gov/data/gridded/data.cobe2.html). The ERA5 reanalysis data are available from https://cds.climate.copernicus.eu/. Radiosonde zonal wind observations for the QBO analysis were obtained from Freie Universität Berlin (https://www.geo.fuberlin.de/en/met/ag/strat/produkte/qbo/index.html).The CESM2 model can be downloaded from https://github.com/ESCOMP/CESM. All data needed to evaluate the conclusions in the paper are present in the paper and/or the Supplementary Materials.

Code availability

The CESM2 model code is freely available from https://github.com/ESCOMP/CESM. The codes for creating the figures and analyses were written in NCAR Command Language Version 6.4. The source codes for the analysis of this study are available from the corresponding author upon reasonable request.

Acknowledgments

We acknowledge the UK Met Office, NOAA (USA), JMA (Japan), ECMWF, the Earth System Grid Federation (ESGF), the CESM project, and Freie Universität Berlin for providing the datasets and observational products used in this study. This work was supported by the National

Natural Science Foundation of China (grant Nos. 42322503, 42361144843, 42175069, 42075052 and 42275056), the Israel Science Foundation (grant no. 3065/23), and the Postgraduate Research & Practice Innovation Program of Jiangsu Province (grant no. KYCX25_1579). The funders were not involved in the study design, data collection, analysis, interpretation of the data, preparation of the manuscript, or the decision to submit the work for publication.

References

1. Anstey JA, *et al.* Impacts, processes and projections of the quasi-biennial oscillation. *Nature Reviews Earth & Environment* **3**, 588-603 (2022).
2. Wang W, Hong J, Shangguan M, Wang H, Jiang W, Zhao S. Zonally asymmetric influences of the quasi-biennial oscillation on stratospheric ozone. *Atmospheric Chemistry and Physics* **22**, 13695-13711 (2022).
3. Koval AV, Gavrilov NM, Kandieva KK, Ermakova TS, Didenko KA. Numerical simulation of stratospheric QBO impact on the planetary waves up to the thermosphere. *Scientific Reports* **12**, 21701 (2022).
4. Anstey JA, *et al.* Teleconnections of the quasi-biennial oscillation in a multi-model ensemble of QBO-resolving models. *Quarterly Journal of the Royal Meteorological Society* **148**, 1568-1592 (2022).
5. Rao J, Garfinkel CI, Ren R, Wu T, Lu Y, Chu M. Projected strengthening impact of the quasi-biennial oscillation on the Southern Hemisphere by CMIP5/6 models. *Journal of Climate* **36**, 5461-5476 (2023).
6. Kang M-J, Kim H, Son S-W. QBO modulation of MJO teleconnections in the North Pacific: impact of preceding MJO phases. *npj Climate and Atmospheric Science* **7**, 12 (2024).

7. Garfinkel CI, Hartmann DL. The influence of the quasi-biennial oscillation on the troposphere in winter in a hierarchy of models. Part II: Perpetual winter WACCM runs. *Journal of the Atmospheric Sciences* **68**, 2026-2041 (2011).
8. Garfinkel CI, Shaw TA, Hartmann DL, Waugh DW. Does the Holton–Tan mechanism explain how the quasi-biennial oscillation modulates the Arctic polar vortex? *Journal of the Atmospheric Sciences* **69**, 1713-1733 (2012).
9. Stockdale TN, *et al.* Prediction of the quasi-biennial oscillation with a multi-model ensemble of QBO-resolving models. *Q J R Meteorolog Soc* **148**, 1519-1540 (2022).
10. Garfinkel CI, *et al.* A QBO cookbook: Sensitivity of the quasi-biennial oscillation to resolution, resolved waves, and parameterized gravity waves. *Journal of Advances in Modeling Earth Systems* **14**, e2021MS002568 (2022).
11. Kim YH, Chun HY. Momentum forcing of the quasi-biennial oscillation by equatorial waves in recent reanalyses. *Atmospheric Chemistry and Physics* **15**, 6577-6587 (2015).
12. Pahlavan HA, Wallace JM, Fu Q, Alexander MJ. Characteristics of gravity waves in opposing phases of the QBO: A reanalysis perspective with ERA5. *Journal of the Atmospheric Sciences* **81**, 1579-1587 (2024).
13. Rao J, Yu Y, Guo D, Shi C, Chen D, Hu D. Evaluating the Brewer–Dobson circulation and its responses to ENSO, QBO, and the solar cycle in different reanalyses. *Earth and Planetary Physics* **3**, 166-181 (2019).
14. Kim YH. Explaining the period fluctuation of the quasi-biennial oscillation. *Atmospheric Chemistry and Physics* **25**, 5647-5664 (2025).
15. Wang Y, Rao J, Lu Y, Ju Z, Yang J, Luo J. A revisit and comparison of the quasi-biennial oscillation (QBO) disruption events in 2015/16 and 2019/20. *Atmos Res* **294**, 106970 (2023).

16. Osprey SM, *et al.* An unexpected disruption of the atmospheric quasi-biennial oscillation. *Science* **353**, 1424-1427 (2016).

17. Kang M-J, Chun H-Y, Son S-W, Garcia RR, An S-I, Park S-H. Role of tropical lower stratosphere winds in quasi-biennial oscillation disruptions. *Science Advances* **8**, eabm7229 (2022).

18. Anstey JA, *et al.* Prospect of increased disruption to the QBO in a changing climate. *Geophysical Research Letters* **48**, e2021GL093058 (2021).

19. Xu W, Ren H-L. Distinct changes in the vertical structure of QBO amplitude due to tropical upwelling and wave forcing. *Environmental Research Letters* **20**, 034014 (2025).

20. Richter JH, *et al.* Progress in simulating the quasi-biennial oscillation in CMIP models. *Journal of Geophysical Research: Atmospheres* **125**, e2019JD032362 (2020).

21. Bushell AC, *et al.* Evaluation of the quasi-biennial oscillation in global climate models for the SPARC QBO-initiative. *Quarterly Journal of the Royal Meteorological Society* **148**, 1459-1489 (2022).

22. Rao J, Garfinkel CI, White IP. Projected strengthening of the extratropical surface impacts of the stratospheric quasi-biennial oscillation. *Geophysical Research Letters* **47**, e2020GL089149 (2020).

23. Santer BD, *et al.* Tropospheric warming over the past two decades. *Scientific Reports* **7**, 2336 (2017).

24. Xie F, Zhang J, Huang Z, Lu J, Ding R, Sun C. An estimate of the relative contributions of sea surface temperature variations in various regions to stratospheric change. *Journal of Climate* **33**, 4993-5011 (2020).

25. Reguero BG, Losada IJ, Méndez FJ. A recent increase in global wave power as a consequence of oceanic warming. *Nature Communications* **10**, 205 (2019).

26. Watanabe M, Dufresne J-L, Kosaka Y, Mauritsen T, Tatebe H. Enhanced warming constrained by past trends in equatorial Pacific sea surface temperature gradient. *Nature Climate Change* **11**, 33-37 (2021).

27. Cheng L, *et al.* Past and future ocean warming. *Nature Reviews Earth & Environment* **3**, 776-794 (2022).

28. Karpechko AY, Manzini E. Arctic stratosphere dynamical response to global warming. *Journal of Climate* **30**, 7071-7086 (2017).

29. Park I-H, Yeh S-W, Min S-K, An S-I, Xie S-P, Shin J. Irreversible changes in the sea surface temperature threshold for tropical convection to CO2 forcing. *Communications Earth & Environment* **5**, 659 (2024).

30. Oberländer-Hayn S, *et al.* Is the Brewer-Dobson circulation increasing or moving upward? *Geophysical Research Letters* **43**, 1772-1779 (2016).

31. Kawatani Y, Hamilton K. Weakened stratospheric quasibiennial oscillation driven by increased tropical mean upwelling. *Nature* **497**, 478-481 (2013).

32. Butchart N, Anstey JA, Kawatani Y, Osprey SM, Richter JH, Wu T. QBO changes in CMIP6 climate projections. *Geophysical Research Letters* **47**, e2019GL086903 (2020).

33. Butchart N. The stratosphere: a review of the dynamics and variability. *Weather Clim Dyn* **3**, 1237-1272 (2022).

34. Bony S, Bellon G, Klocke D, Sherwood S, Fermepin S, Denvil S. Robust direct effect of carbon dioxide on tropical circulation and regional precipitation. *Nature Geoscience* **6**, 447-451 (2013).

35. Sigmond M, Siegmund PC, Manzini E, Kelder H. A simulation of the separate climate effects of middle-atmospheric and tropospheric CO2 doubling. *Journal of Climate* **17**, 2352-2367 (2004).

36. He J, Soden BJ. Anthropogenic weakening of the tropical circulation: The relative roles of direct CO2 forcing and sea surface temperature change. *Journal of Climate* **28**, 8728-8742 (2015).

37. Kodama C, Iwasaki T, Shibata K, Yukimoto S. Changes in the stratospheric mean meridional circulation due to increased CO2: Radiation- and sea surface temperature–induced effects. *Journal of Geophysical Research: Atmospheres* **112**, (2007).

38. Kawatani Y, Hamilton K, Noda A. The effects of changes in sea surface temperature and CO2 concentration on the quasi-biennial oscillation. *Journal of the Atmospheric Sciences* **69**, 1734-1749 (2012).

39. DallaSanta K, Orbe C, Rind D, Nazarenko L, Jonas J. Dynamical and trace gas responses of the Quasi-Biennial Oscillation to increased CO2. *Journal of Geophysical Research: Atmospheres* **126**, e2020JD034151 (2021).

40. Fosu B, He J, Liguori G. Equatorial Pacific Warming Attenuated by SST Warming Patterns in the Tropical Atlantic and Indian Oceans. *Geophysical Research Letters* **47**, e2020GL088231 (2020).

41. Serva F, Cagnazzo C, Christiansen B, Yang S. The influence of ENSO events on the stratospheric QBO in a multi-model ensemble. *Climate Dynamics* **54**, 2561-2575 (2020).

42. Naoe H, *et al.* QBOi El Niño–Southern Oscillation experiments: teleconnections of the QBO. *Weather Clim Dynam* **6**, 1419-1442 (2025).

43. Kawatani Y, *et al.* QBOi El Niño–Southern Oscillation experiments: overview of the experimental design and ENSO modulation of the QBO. *Weather Clim Dynam* **6**, 1045-1073 (2025).
44. Zhu X, Rao J. Possible coherency of synchronous warming of tropical oceans and the QBO amplitude variation. *Atmospheric Research* **325**, 108241 (2025).
45. Richter JH, *et al.* Response of the quasi-biennial oscillation to a warming climate in global climate models. *Quarterly Journal of the Royal Meteorological Society* **148**, 1490-1518 (2022).
46. Zhou T, *et al.* Exploring the ENSO modulation of the QBO periods with GISS E2.2 models. *Atmospheric Chemistry and Physics* **24**, 509-532 (2024).
47. Kawatani Y, Hamilton K, Sato K, Dunkerton TJ, Watanabe S, Kikuchi K. ENSO modulation of the QBO: Results from MIROC models with and without nonorographic gravity wave parameterization. *Journal of the Atmospheric Sciences* **76**, 3893-3917 (2019).
48. Serva F, *et al.* The impact of the QBO on the region of the tropical tropopause in QBOi models: Present-day simulations. *Q J R Meteorolog Soc* **148**, 1945-1964 (2022).
49. Dong Y, Polvani LM, Hwang Y-T, England MR. Stratospheric ozone depletion has contributed to the recent tropical La Niña-like cooling pattern. *npj Climate and Atmospheric Science* **8**, 150 (2025).
50. Kang JM, Thomas R, Dunstone N, Shaw TA, Woollings T. Robust impact of tropical Pacific SST trends on global and regional circulation in boreal winter. *npj Climate and Atmospheric Science* **8**, 315 (2025).
51. Li X, Xie S-P, Gille ST, Yoo C. Atlantic-induced pan-tropical climate change over the past three decades. *Nature Climate Change* **6**, 275-279 (2016).

52. Jiang L, Li T. Impacts of tropical North Atlantic and equatorial Atlantic SST anomalies on ENSO. *Journal of Climate* **34**, 5635-5655 (2021).

53. Holt LA, *et al.* An evaluation of tropical waves and wave forcing of the QBO in the QBOi models. *Quarterly Journal of the Royal Meteorological Society* **148**, 1541-1567 (2022).

54. Franke H, Preusse P, Giorgetta M. Changes of tropical gravity waves and the quasi-biennial oscillation in storm-resolving simulations of idealized global warming. *Quarterly Journal of the Royal Meteorological Society* **149**, 2838-2860 (2023).

55. He Y, Zhu X, Sheng Z. Dynamic configuration before quasi-biennial oscillation disruptions revealed from the perspective of planetary waves. *npj Climate and Atmospheric Science* **8**, 79 (2025).

56. Wang Y, Rao J, Lu Y, Ju Z. QBO disruption–like events in the China Meteorological Administration climate model. *Advances in Atmospheric Sciences* **42**, 1813-1832 (2025).

57. Rayner NA, *et al.* Global analyses of sea surface temperature, sea ice, and night marine air temperature since the late nineteenth century. *Journal of Geophysical Research: Atmospheres* **108**, (2003).

58. Huang B, *et al.* Extended reconstructed sea surface temperature, version 5 (ERSSTv5): Upgrades, validations, and intercomparisons. *Journal of Climate* **30**, 8179-8205 (2017).

59. Hirahara S, Ishii M, Fukuda Y. Centennial-scale sea surface temperature analysis and its uncertainty. *Journal of Climate* **27**, 57-75 (2014).

60. Naujokat B. An update of the observed quasi-biennial oscillation of the stratospheric winds over the tropics. *Journal of Atmospheric Sciences* **43**, 1873-1877 (1986).

61. Hersbach H, *et al.* The ERA5 global reanalysis. *Quarterly Journal of the Royal Meteorological Society* **146**, 1999-2049 (2020).

62. Eyring V, *et al.* Overview of the coupled model intercomparison project phase 6 (CMIP6) experimental design and organization. *Geosci Model Dev* **9**, 1937-1958 (2016).

63. Simpson IR, *et al.* An evaluation of the large-scale atmospheric circulation and its variability in CESM2 and other CMIP models. *Journal of Geophysical Research: Atmospheres* **125**, e2020JD032835 (2020).

64. Rao J, Ren R. A decomposition of ENSO's impacts on the northern winter stratosphere: competing effect of SST forcing in the tropical Indian Ocean. *Climate Dynamics* **46**, 3689-3707 (2016).

65. Rao J, Ren R. Varying stratospheric responses to tropical Atlantic SST forcing from early to late winter. *Clim Dyn* **51**, 2079-2096 (2018).

66. Wallace JM, Panetta RL, Estberg J. Representation of the equatorial stratospheric quasi-biennial oscillation in EOF phase space. *Journal of Atmospheric Sciences* **50**, 1751-1762 (1993).

67. Kumar V, Hitchman MH, Du W, Dhaka SK, Yoden S. Teleconnection of the Quasi-biennial oscillation with boreal winter surface climate in Eurasia and North America. *Commun Earth Environ* **5**, 251 (2024).

68. Andrews DG, Leovy CB, Holton JR. *Middle atmosphere dynamics*. Academic press (1987).

69. Pahlavan HA, Fu Q, Wallace JM, Kiladis GN. Revisiting the quasi-biennial oscillation as seen in ERA5. Part I: Description and momentum budget. *Journal of the Atmospheric Sciences* **78**, 673-691 (2021).

70. Pahlavan HA, Wallace JM, Fu Q, Kiladis GN. Revisiting the quasi-biennial oscillation as seen in ERA5. Part II: Evaluation of waves and wave forcing. *Journal of the Atmospheric Sciences* **78**, 693-707 (2021).

71. Latif M, *et al.* Strengthening atmospheric circulation and trade winds slowed tropical Pacific surface warming. *Communications Earth & Environment* **4**, 249 (2023).

Author contributions

Y.W. and J.R. conceived the study and developed the methodology. Y.W. conducted the investigation and performed the formal analysis. Y.W. prepared the figures and visualizations. J.R., C.I.G., and R.R. supervised the research. Y.W. wrote the original draft of the manuscript. J.R., C.I.G., R.R., S.M.O., and Y.L. reviewed and edited the manuscript. All authors have read and approved the manuscript.

Competing interests

The authors declare no competing financial or non-financial interests.